

# GigaGauss magnetic fields in under-dense plasma

Zs. Lécz, I. V. Konoplev, A. Seryi, A. Andreev

December 3, 2024

Magnetic fields have a crucial role in physics at all scales, from synchrotrons and laser-driven plasma accelerators to astrophysics and nanotechnology. Large field strengths, beside the guiding of relativistic particles along a shorter curvature, allows the investigation of material in extreme conditions existing only in exotic astro-objects like neutron stars or pulsars. Here we propose a method for generating magnetic field on the GigaGauss level in under-dense plasma using high intensity laser pulses with azimuthally non-uniform intensity distribution. The interaction is studied with the help of three-dimensional particle-in-cell plasma simulation code. Beside the standard wake-field and bubble generation, such laser beam induces the rotational motion of electrons at the edge of evacuated plasma region. The combined axial magnetic and electric fields form a compact source of both high frequency radiation, due to coherent synchrotron emission, and low emittance, high density relativistic electron bunches. We will also discuss the regime at which static solenoidal field can be observed without electron acceleration with longer life-time but smaller magnetic field amplitude.

## 1 Introduction

Magnetic field is one of the fundamental entities which influence nature on all scales. It shapes planets and stars [1], electron beams in particle accelerators are guided and focused by magnetic fields [2] and it is used to understand natural phenomena under extreme conditions [3]. Magnetic field is used to stimulate coherent x-ray radiation from charged particle beams [4] and it is responsible for the most spectacular natural phenomena i.e. Aurora Borealis. A capability to generate high strength magnetic field is essential for many project and research communities (see for example MegaGauss International conferences). The magnetic fields of MegaTesla level strength are observed for example inside neutron stars [5] and can be used to understand some other astrophysical phenomena [6, 3] as well as matter behavior under extreme conditions [7]. The fields of up to 1kT strength are currently generated using explosive magnetic generators [8] or high-current single short targets driven by pulsed power generators [9] which are used to generate high intensity X-ray fluxes. Such machines are capable of generating magnetic fields of high strength (140 T) [10] and there are prediction of possible generation of up to 600 T in some cases [11]. The single shot techniques are well developed and allows generating of fields around 1kT. Alternatively if non destructive machines are used the maximum strength field achieved using solenoids (without solenoid destruction) is reported to be 100T at Los Alamos National Laboratory [12]. Reaching magnetic fields of a GigaGauss strength levels seems to be impossible as electron currents which is required to drive such fields and  $\mathbf{J} \times \mathbf{B}$  self induced forces will destroy any currently available material. In order to resolve these problems we suggest to generate magnetic fields of GigaGauss strength level inside cubic volume of  $10s \mu m$  dimensions in femtosecond time scale. This field is generated in under-dense plasmas and can be driven either by angular rotating (screw-like) laser [16] or electron beams. In this paper we will focus on the laser beams driven magnetic field while the excitation of the field by the charge particles will be considered in the following studies.

In under-dense plasmas to generate the high-strength magnetic fields a solenoid like currents can be excited by high intensity laser beam with an angular momentum [16, 17]. In particular a screw-shaped laser pulse is considered for efficient transfer of orbital angular momentum to the

electrons in plasma [16]. One notes that generation of such laser beams is interesting topic in its own right [17] and we assume that it can be generated via compression/focusing along a single rotating plane of circular polarized beam or shaping it with relativistic electrons [14, 15] and amplifying the generated higher harmonics [17]. In this paper we have identified and will consider two operating regimes under which magnetic field can be generated, namely: bubble solenoid and steady solenoid regimes. In the first regime the magnetic field is generated by the electron currents moving around plasma bubble shell in a similar to solenoid manner with the highest field observed at the end of the bubble where electrons trajectories are collapsing creating high strength magnetic field. In this case the field's strength is adiabatically changing from the center of the bubble to its end reaching the highest amplitude. The magnetic field direction coincides with the direction of laser propagation with the volume (few cubic micrometers) having the highest field, defined by the step of the laser spiral. The second regime is realized when a set of conditions (discussed below in the paper) are such that the plasma bubble is not formed and the solenoid currents are not limited to the dimensions of the bubble. In this case the field can be sustained over longer distances (around  $100s\mu m$ ) but the field amplitude achieved in this regime will be order of magnitude less (i.e.  $10s\text{ kT}$ ).

The paper is structured as follow: the second section is dedicated to the model description while in the third section different regimes will be considered. In the conclusion we discuss the results and outline future work and possible impacts. We note that here we will only assume one of possible applications of such fields namely to reduce the emittance of the electron bunch in laser plasma acceleration. However it is clear that the capability to generate such fields will allow dramatic progress in non-destructive, reproducible studies of phenomena at fields strength which are not yet accessible in the laboratories.

## 2 Electron blow-out and collapse

The laser-plasma (LP) interaction is one of the most dynamic research areas which is driven by number of problems including design of compact light sources and particle accelerators. Another challenge, which can be resolved using LP interaction is generation of magnetic fields of MegaTesla (MT) strength. One notes that to resolve this problem the laser-plasma parameters should be different from ones used in conventional studies [21] and in general may not be optimal for example for LP acceleration of electrons.

Let us consider that for the condition  $\lambda_p \gg \lambda_L$ , where  $\lambda_p = 2\pi c/\omega_p$  is the plasma wavelength with  $\omega_p = (n_0 e^2 / (\gamma m_e \epsilon_0))^{1/2}$  (relativistic plasma frequency, where  $n_0$  is the unperturbed plasma density,  $\gamma$  and  $m_e$  is the relativistic factor and mass of electron) and  $\lambda_L$  is the laser wavelength, the electrons feel the average ponderomotive force of the pulse, which is proportional to the gradient of the intensity defined by the envelope function [18, 19]. This is well known laser envelope model which is widely used for investigation of laser wake field acceleration (LWFA) in low density plasmas [20]. This is appropriate and valid "short-cut" to minimise the spatial resolution of numerical modeling which leads to reduction of calculation time. We use a similar model (see Appendix) and the same concept for studying the effect of laser pulse shape and its angular momentum on the bubble formation and magnetic field generation. We note that the 3D models of these phenomena have been studied using 3D Particle in Cell (PIC) code VSim and results presented here are observed using this code.

The exact analytical description of the laser pulse is presented in the Appendix. The laser pulse shape i.e. its envelope function, illustrated in Fig. 1a, is similar to a drill bit propagating along x-coordinate and Fig. 1b shows the electron dynamics while the pulse propagates through the plasma. One notes that the main difference (in plasma dynamics) between the standard Gaussian and the spiral-shaped beam propagation through the plasma is the azimuthal non-uniformity of electron density (i.e. appearance of azimuthal current) along the bubble surface.

The electrons expelled by the laser pulse will move along spiral trajectories on the surface of the generated bubble (azimuthal electron current), which in turn induces strong axial magnetic field with the maximum value in the back of the bubble. Indeed the spiral shaped laser pulse

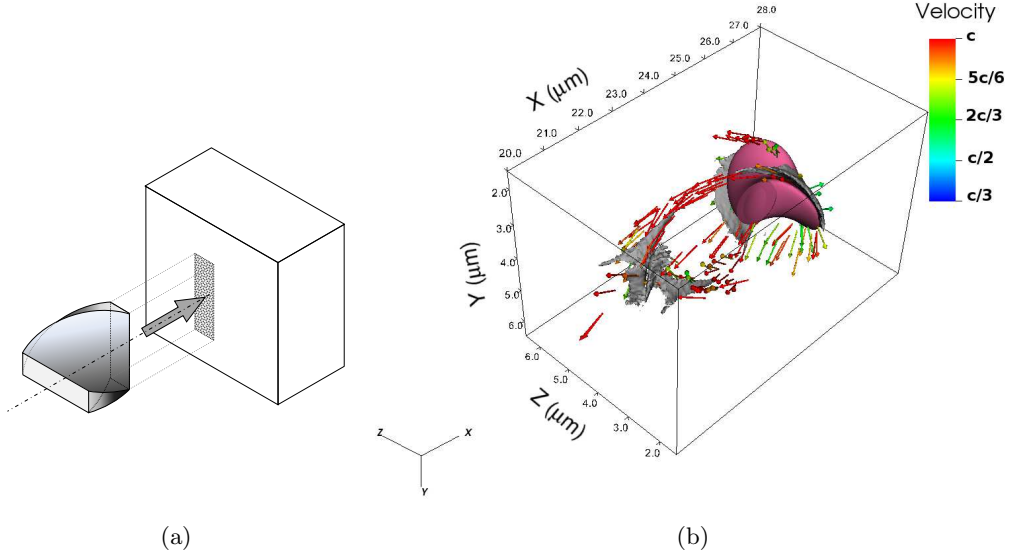


Figure 1: (a) Schematic of the laser pulse moving into the plasma (grey box) with momentary projection of the pulse front on the box. The projection rotates in time and (b) illustrates the isosurface of pulse intensity (purple) at the value of  $2 \times 3 \times 10^{20} \text{ W/cm}^2$  and electron density (gray) with  $10^{26} \text{ m}^{-3}$ . The arrows represent the velocity vectors of electrons seen from the moving frame of the laser pulse and the color code shows their magnitude.

gives a twist to the electrons which can be seen at the right side of Fig. 1b (in the vicinity of the pulse). As they travel to the back side of the bubble two electric current channel are formed, which approach each other and finally pass by within a distance less then laser spot diameter. The currents cannot merge as these two electron currents have opposite direction, repelling each other and thus limiting the magnetic field generated at the merging point. However, the maximum value of the field is generated at the end of the bubble due to the fact that the electrons' trajectories are approaching each other in this region. This motion as well as dense electron bunches are shown in Fig. 1b. Let us note that in order to minimize the calculation time and for better illustration of the electron currents we move to the frame co-moving with the laser pulse. This is possible under the assumption that the phenomena described is strongly localized (in time space frame) and there is no feedback from the outside the frame. We also note that throughout the paper the laser wavelength is adjusted such that the conditions  $\lambda_L \ll \lambda_{sp}$ , where  $\lambda_{sp}$  is the spiral step, and  $n_0 < n_{cr}$ , where  $n_{cr} = \omega_L^2 m_e \epsilon_0 / e^2$ , are fulfilled.

In the example shown in Fig. 1b the peak intensity is  $I_0 = 1.6 \times 10^{21} \text{ W/cm}^2$ , the pulse width is  $1.8 \mu\text{m}$  (FWHM), the pulse length is equal to the spiral step,  $\lambda_{sp} = 1.8 \mu\text{m}$ , and electron density is typical fully ionized C-H gas density,  $n_0 = 0.62 \times 10^{-3} n_{cr} = 7 \times 10^{25} \text{ m}^{-3}$ . In order to use our envelope model the plasma has to be strongly underdense, i.e.  $n_0/n_{cr} \ll 1$ , to ignore the pulse energy depletion and if higher densities plasmas is studied the pulse depletion is significant and should be taken into consideration (see Appendix).

The complex dynamics of electrons fluxes and mechanism of the field generation is more elucidated in Fig. 2a, where the electron streamlines are shown flowing around the bubble in three dimensions. On the lateral sides of the simulation box the cross sections of the longitudinal magnetic field are shown, which are taken along the axis of the propagation. The back side presents the transversal cross section of the electron density at the tail of the bubble. In the right picture of Fig. 2b a more detailed structure of the electric currents is shown. Here one sees that a part of the electron tracks simply pass through and leave the highly concentrated region while some electrons will be captured by the electromagnetic (EM) potential and start to move on a spiral path around the axial magnetic field. A small portion of the electrons moves a outward and will

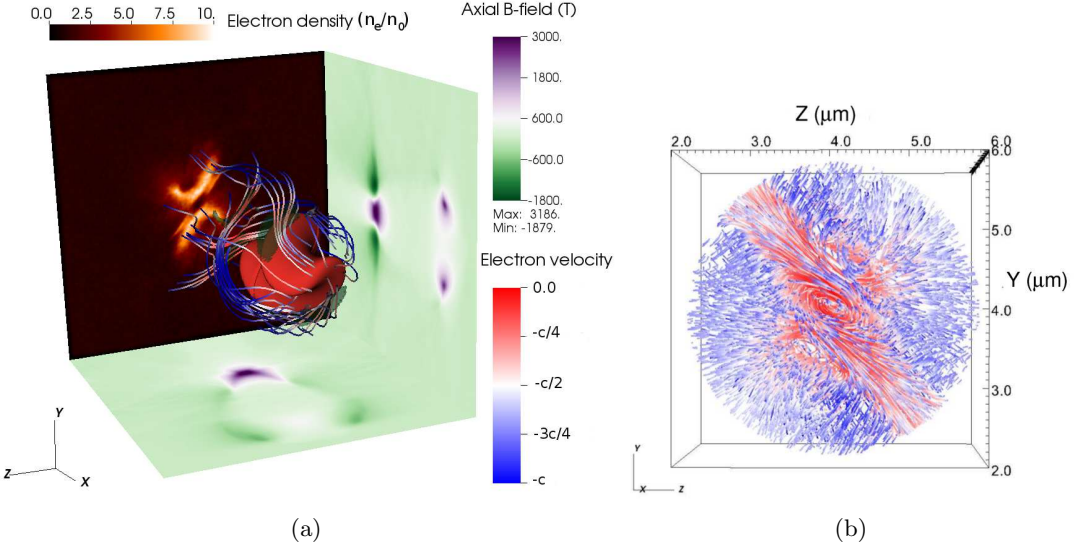


Figure 2: (a) Three-dimensional view of the electron streamlines. On the faces of the visualization box the cross section of axial magnetic field and charge density of electrons are shown. The transparent green isosurface illustrates the regions where the electric current is the highest. (b) Zoom on the streamlines in the back of the bubble. The color code is the same as in the left picture.

spiral in the opposite direction because of the negative B-field seen in the  $xy$  plane of the left picture.

The electron trajectory and bubble shape strongly depends on the balance between the kinetic energy of electrons gained in the force field of the laser pulse and on the EM potential generated by the bubble where the electrons are evacuated from. If the latter is high enough, electrons are captured and accelerated while moving in the strong magnetic field. This electron dynamics can be beneficial for improving an accelerated electron beam emittance in laser plasma accelerators. The internal structure of the longitudinal magnetic field depends on the number of captured electrons and for example if the bubble size is large or plasma density is high while the laser parameters are not adjusted correctly, the efficiency of B-field generation decreases.

### 3 Magnetic field structure and scaling with parameters

#### 3.1 The bubble solenoid

Let us consider the case when the majority of the collapsing at the end of the bubble electrons can escape the attracting field of the bubble and do not disturb the generated magnetic field. Here we will consider the dependance of the magnetic field on following set of laser and plasma parameters: plasma density, laser pulse spiral step, intensity, and the wavelength. All these parameters define the electron currents outside the bubble which drive the MT level magnetic field. In order to check the dependence on the spiral step the following simulations were performed, with the results presented in Fig. 3. In all cases the pulse length is equal to the half of the pulse spiral step, which means 180 degrees rotation of the intensity profile (Fig.1a). It can be clearly seen that as the pulse length becomes comparable with the bubble size the magnetic field profile gets more similar to a solenoid in the  $xz$  plane. The peak axial magnetic field is more localized in the case of short  $\lambda_{sp}$ , while it is more elongated in the case of larger  $\lambda_{sp}$ . In the left panels of Fig. 3 the normalized electron density distribution is shown. It is clear that the charge densities in  $xy$  and  $xz$  planes are different as a result of "asymmetric" laser pulse. Higher compression is visible for the smaller

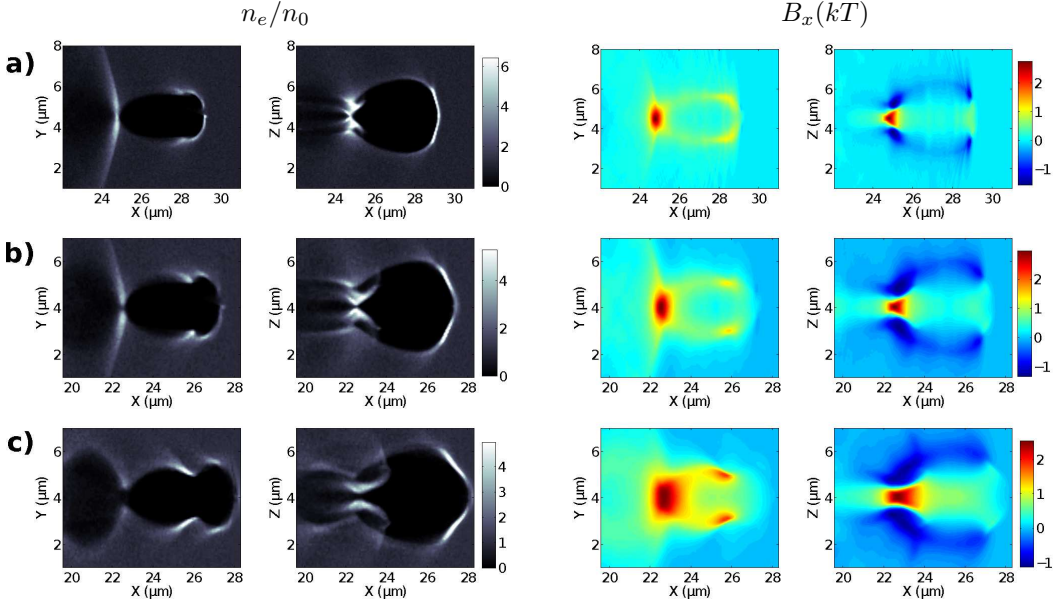


Figure 3: Cross sections of electron density normalized to initial density in the two orthogonal transversal planes and the corresponding magnetic fields in the same planes for rows: a)  $\lambda_{sp} = 0.9\mu\text{m}$ ; b)  $1.8\mu\text{m}$ ; and c)  $3.6\mu\text{m}$ . In all cases  $n_0 = 0.62 \times 10^{-3}n_{cr}$ .

spiral step, however a slightly higher peak of magnetic field was observed for intermediate value of spiral step, which is shown in Fig. 4. This may be an indication of development of more complex electrons dynamics which is also driven by self-induced fields rather than only under the influence of the external forces.

|      | $2\sigma_1$ (μm) | $\lambda_L$ (nm) | $I_0$ (W/cm <sup>2</sup> ) | $n_0/n_{cr}$          | $\max(B_x)$ (T)    |
|------|------------------|------------------|----------------------------|-----------------------|--------------------|
| Sim1 | 1.8              | 100              | $1.6 \times 10^{21}$       | $0.62 \times 10^{-3}$ | 3000               |
| Sim2 | 1.2              | 100              | $8 \times 10^{21}$         | $6.2 \times 10^{-3}$  | $2.8 \times 10^4$  |
| Sim3 | 0.8              | 100              | $3.2 \times 10^{22}$       | 0.062                 | $2.5 \times 10^5$  |
| Sim4 | 0.3              | 20               | $8 \times 10^{23}$         | 0.025                 | $0.95 \times 10^6$ |
| Sim5 | 14.4             | 800              | $1.6 \times 10^{21}$       | 0.04                  | $1.2 \times 10^4$  |
| Sim6 | 14.4             | 800              | $0.8 \times 10^{21}$       | 0.01                  | 5000               |
| Sim7 | 14.4             | 800              | $3.2 \times 10^{21}$       | 0.01                  | 9000               |
| Sim8 | 9.6              | 800              | $2 \times 10^{22}$         | 0.1                   | $5 \times 10^4$    |

Table 1: Simulation parameters. For simulations 1-4  $\lambda_{sp} = 0.9\mu\text{m}$ , except Sim4 where  $\lambda_{sp} = 0.3\mu\text{m}$ , and for 5-8  $\lambda_{sp} = 7.2\mu\text{m}$ . In all simulations  $\sigma_2 = \sigma_1/2$ .

Indeed the shape of the magnetic field distribution and the actual peak value depend on the details of complex electron's trajectories and on the compression level which they acquire in the tail of the bubble. However the self induced repulsive forces can result in destruction of the currents and thus limiting the amplitude of generated magnetic field. If we assume that the transversal size of the bubble does not change (which is true in Fig. 3) the compressed electron density scales as  $n_e = (\lambda_p/\lambda_{sp})n_0$ . The second thing to be noticed is the fact that the magnetic field is generated by finite current sheets with thickness approximately  $\lambda_{sp}/2$ . Applying Ampere's law to this geometry one finds for the magnetic field  $B = \mu_0 j_0 \lambda_{sp}$ , where  $j_0 = e n_e v_\varphi$  and  $v_\varphi$  is the azimuthal velocity. Inserting the expression for the compressed electron density and considering that some of the evacuated electrons contribute to the transversal current we find  $B = p \mu_0 e n_e \lambda_p v_\varphi / 2$ , where  $p < 1$  indicates the percentage of electrons contributing to the transverse current. If one uses  $\lambda_p \approx 8\mu\text{m}$

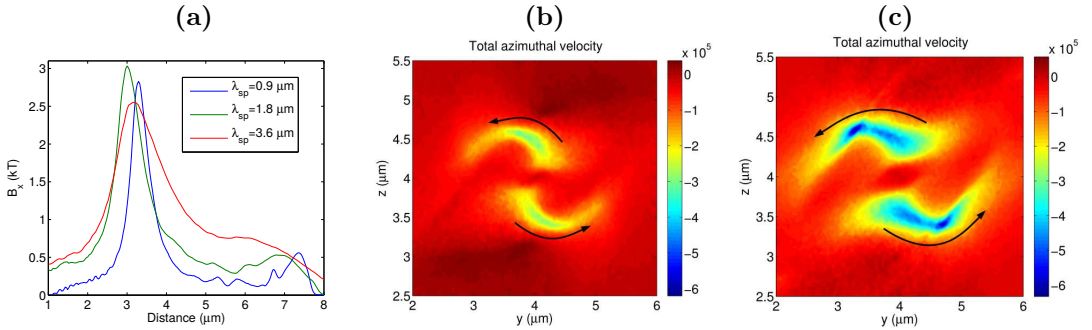


Figure 4: a) Longitudinal magnetic field along the axis of propagation for different spiral steps of the laser pulse presented in Fig. 3. b) and c) show the total azimuthal velocity ( $\sum v_\varphi/c$ ) distribution in the transverse plane at the back of the bubble for  $\lambda_{sp} = 0.9\mu\text{m}$  and  $\lambda_{sp} = 3.6\mu\text{m}$ , respectively. The negative velocity (blue colors) indicates clockwise rotation while small positive or near zero velocities (red colors) indicates anti-clock rotation. The circle indicates the area of high compression where the highest magnetic field amplitude is achieved

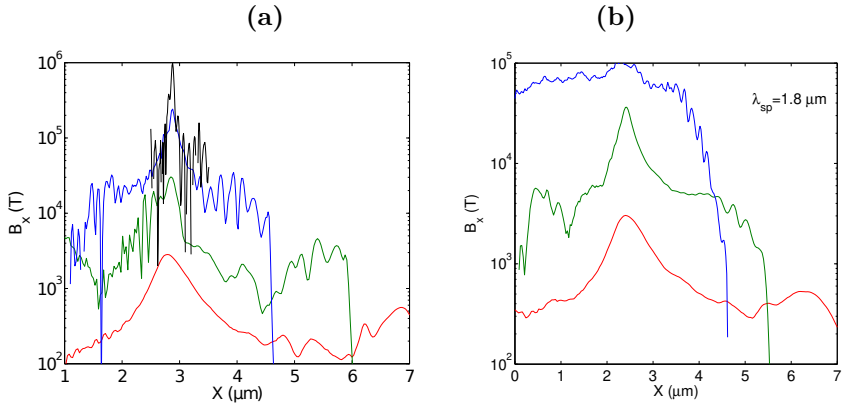


Figure 5: Longitudinal magnetic field along the axis of propagation for parameters shown in: (a) Table 1 and (b) for two times larger spiral step. The red, green, blue and black lines corresponds to simulations 1, 2, 3, 4 respectively. The color code is the same in both pictures.

the estimated value of the B-field is  $B \approx p \cdot 16 \text{ kT}$ , which is close to the measured one if assume that only quarter of the electrons are contributing to the transverse current.

Seemingly the peak magnetic field does not depend on the spiral step (or pulse length), but through the expression of ponderomotive force we find that  $\gamma \sim \nabla I_L \lambda_L^2 \sim I_0 \lambda_L/l$ , where  $l = \lambda_{sp}/\lambda_L$ . On the other hand the bubble length (or half plasma wavelength) is proportional to  $\sqrt{\gamma/n_0}$ , thus  $B \sim (\gamma n_0)^{1/2} v_\varphi$ . This scaling indicates that the axial magnetic field shown in Fig. 4a should be two times lower for 4 times longer spiral step. However, the peak values are almost the same, which can be attributed to the larger azimuthal momentum acquired with larger  $\lambda_{sp}$ . The comparison of azimuthal velocity distribution in the back of the bubble is shown in Fig. 4b and 4c for  $\lambda_{sp} = 0.9\mu\text{m}$  and  $\lambda_{sp} = 3.6\mu\text{m}$ , respectively. The number of rotating electrons is the same in both cases, but their azimuthal velocity is two times higher in the case of longer spiral step, which compensates for the reduced gamma factor.

It is straightforward to expect higher magnetic field for a longer time intervals and thus inside larger volumes by increasing the laser intensity (energy available to drive the current) and plasma density (current available to generate the field). In the following studies it is proven that with the laser intensity reachable with the current technology the MT level magnetic fields can be generated in the experiments in the laboratory environment. The parameters used in the next simulations

are shown in Table 1. The first parameter-set (Sim1) has been used in the previous simulations. The bubble size is defined by three parameters: laser spot size ( $W_L = 2\sigma_1$ ), laser intensity and plasma density. In order to have similar bubble structure as before we chose the laser spot size to be between one third and half of the bubble length.

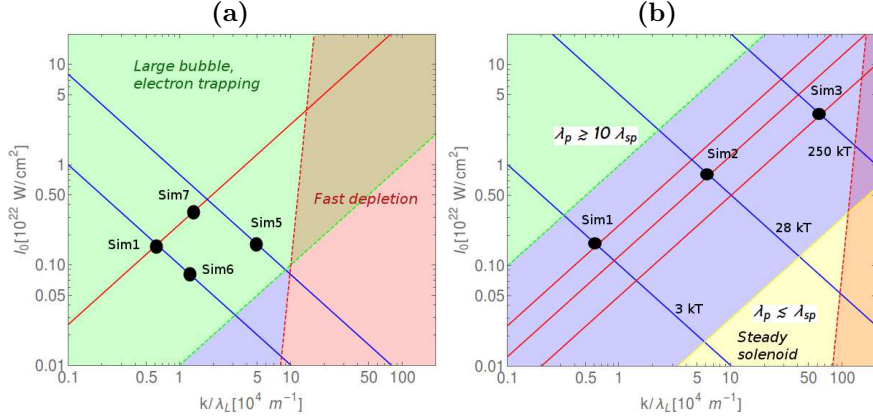


Figure 6: Parameter-map of the mechanism, where the region of different regimes are also indicated, for two laser wavelengths: a)  $\lambda_L = 800$  nm and b)  $\lambda_L = 100$  nm. The blue and red lines show the parameters required to generate the same magnetic field amplitude and the same field distribution, respectively. The blue area shows the parameter interval discussed in this section: the bubble solenoid regime. The red dashed line corresponds to  $k = n_0/n_{cr} = 0.1$ , behind which the laser pulse depletion affects the magnetic field generation and the model should be revisited.

The axial magnetic fields measured for the first four parameter-sets are shown in Fig. 5a and 5b. The expression derived above, in the strongly relativistic case, i.e.  $v_\varphi \approx c$ , predicts a scaling  $B \sim (\gamma n_0)^{1/2}$ , which is close to the observed scaling. In the case of larger spiral step (Fig. 5b) the third simulation did not give the expected result, because the pulse was longer than the bubble and the magnetic field generation enters a different regime, discussed later. In the case of Sim4 the plasma density is near the solid density, which allows the formation of very small bubble, therefore the laser wavelength and pulse size had to be decreased. Although the resulting magnetic field reaches the MT level, the required laser parameters do not seem to be reachable at the current stage of laser technology. However, it is possible to scale the parameters such that the resulting B-field remains the same. For this the following condition has to be fulfilled:  $n_0 \lambda_p \approx \text{constant}$ , which is equivalent to  $\sqrt{n_0 I_0 \lambda_L / l} \sim \sqrt{k I_0 / (\lambda_L l)} \approx \text{constant}$ , where  $k = n_0 / n_{cr}$ . In order to have the same bubble shape the following constrain can be added:  $\lambda_p / \lambda_{sp} \sim \sqrt{I_0 / (\lambda_L l^3 n_0)} \sim \sqrt{I_0 \lambda_L / (l^3 k)} \approx \text{constant}$ . Unfortunately by increasing the laser wavelength up to  $0.8 \mu\text{m}$  the plasma becomes overdense which results in quick depletion (or absorption) of the laser pulse and no axial B-field is generated (see supplementary material). At this stage we can speculate that the issue can be resolved if for instance an electron beam with angular momentum is used to drive the currents capable of generating MT magnetic fields.

From the expressions presented above it follows that either the bubble shape or magnetic field amplitude changes by modifying the laser or plasma parameters. In the above simulations the dimensionless pulse length was  $l = 9$  and if it is kept the same, the laser wavelength and intensity can be tuned, within well defined limits, to obtain the same magnetic field strength. In Fig. 6 the iso-value curves of  $\max(B_x)$  and  $\lambda_p / \lambda_{sp}$  are shown, which indicate the parameter plane scaling for constant pulse length  $l$ . The simulations discussed and presented in Table 1 are shown on these planes of parameters. The blue area indicates the parameter space where the bubble regime (discussed in this section) can be observed. The green area shows the regime of strong electron trapping (not favorable for generation of large magnetic fields), the yellow area corresponds to the regime of steady solenoid (presented in the next section) and the red area is the area where the plasma density is large enough resulting in the laser pulse energy depletion to become not

negligible on our time scale of the interest. It is clearly visible that the laser wavelength strongly influences the diagram and it pushes the blue area towards lower intensity and density regions, which in turn means weaker magnetic field generation. One notice that for the generation of high B-field in static bubble solenoid high intensity and short wavelength is required.

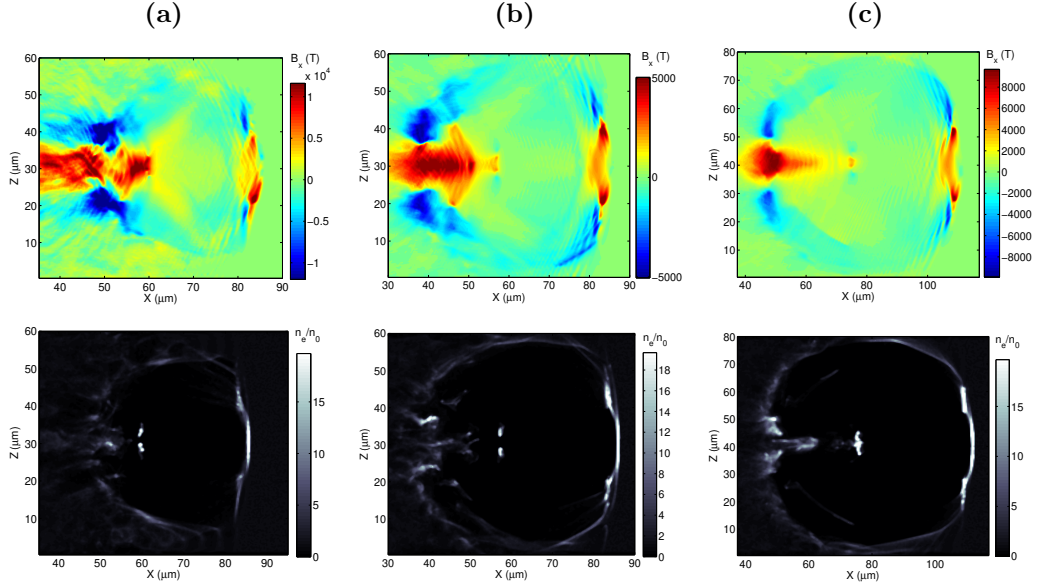


Figure 7: Longitudinal magnetic generated in the upper row and normalized electron density in the lower row observed for the parameter sets shown in Table 1: (a) Sim5, (b) Sim6 and (c) Sim7.

In order to prove the validity of the scalings we show the magnetic field cross sections from simulation 5, 6, 7 in Fig. 7, where the laser wavelength is 8 times longer than in Sim1. It can be clearly seen that by increasing only the laser wavelength the field amplitude increases by  $\approx \sqrt{8}$ , but the relative size of the bubble does decreases by the same factor (compare Fig. 7a to Fig. 3c). This can be attributed to the large amount of captured electrons, which decrease the electrostatic potential inside of the bubble, leading to its expansion. The laser intensity and plasma density can be changed such that almost the same magnetic field is obtained (Sim6) and the ratio  $\lambda_p/\lambda_{sp}$  becomes larger (Fig. 7b). Finally the same bubble shape can be obtained by increasing the laser intensity and decreasing the plasma density (Sim7).

Plasma waves produced in the under-dense plasmas are famous for their capability of accelerating electrons to GeV energy. This is also true in the case of screw-like-shape of the laser pulses. In this case the longitudinal accelerating field is combined with strong longitudinal magnetic field which is pointing in the same direction giving set of new features to this accelerating scheme. Due to the B-field produced in the tail of the bubble very large number of electrons can be accumulated in the accelerated beam with dramatically improved emittance. In case shown in Fig. 8 the electron energy has reached the 400 MeV after only 50 μm of propagation. It is clear that this high energy is due to the high plasma density and high laser intensity used in the simulation. The energy spectrum and angular distribution of electrons is shown in Fig. 8. Even at this preliminary studies an efficient acceleration and multiple beam bunching is visible. In Fig. 8a three electron bunches are formed which are distinguishable in Fig. 8e,f. As their energy increases their angular spread decreases and probably will be unified into a single dense and energetic electron bunch if the acceleration is long enough. The energy spread of electrons is relatively large, but the angular spread of the individual bunches is less than 1 mrad.

Due to the strong magnetic field these electrons are compressed, and rotate along the magnetic field lines. This electron beam dynamics can be very interesting for generating high intensity synchrotron radiation (SR) at  $< \text{nm}$  wavelength scale predominantly in the forward direction. Since the spatial resolution of our simulation method is not high enough to resolve these wavelengths

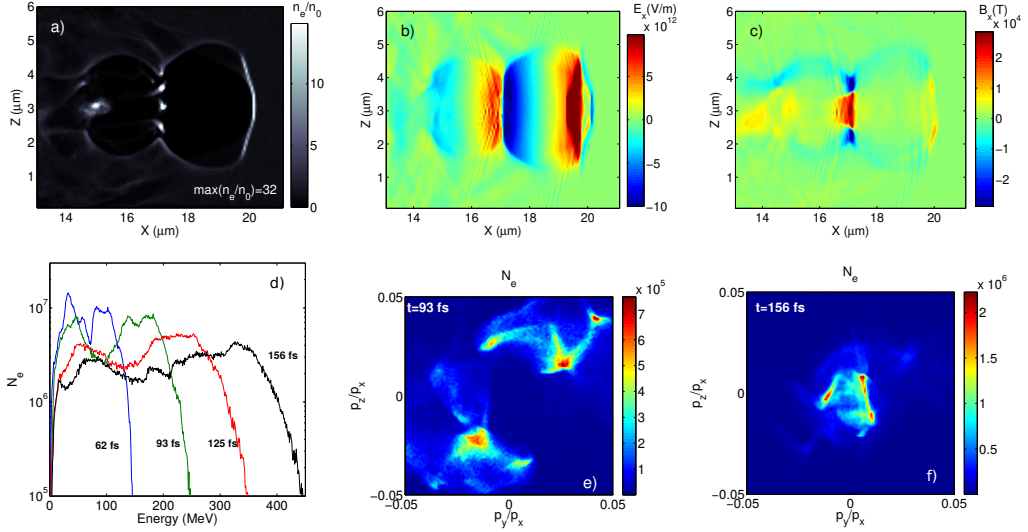


Figure 8: (a) A snapshot of electron density, (b) longitudinal electric field and (c) axial magnetic field in the case of Sim2. (d) Electron energy and (e,f) momentum distributions for different time instances.

(and the spiral motion of electrons) this radiation can not be investigated at this stage of the numerical modeling and will be studied in the future. We anticipate that due to electron spiral motion in magnetic field strong energy loss from the transversal motion will take place due to intense SR. The SR losses per unit length are [22]:

$$\frac{dW}{dS} = \frac{2}{3} \frac{r_e \gamma^4 m_e c^2}{R^2}, \quad (1)$$

where  $r_e$  is the classical electron radius and  $R$  is the radius of curvature of electron motion defined by the magnetic rigidity,  $B\rho$ [Tm]  $\approx 3.33p$ [GeV/c], and azimuthal angle of electron motion,  $\theta$ :  $R = \theta B\rho / B_x$ . The derivation in the above expression can be transformed as  $dW/dS = dS/dx(dW/dx) = \theta dW/dx$ . Let us define the cooling length  $L_{cool}$  to be equal to the distance over which the electron will lose all its energy due to SR. Since the electron continue to receive acceleration in longitudinal direction, its transverse emittance will decrease by a factor of  $e = 2.718$  over  $L_{cool}$ :

$$L_{cool} = \frac{3}{2} \frac{R^2}{r_e \gamma^3 \theta} = \frac{3}{2} \left( \frac{B\rho}{B_x} \right)^2 \frac{\theta}{r_e \gamma^3}. \quad (2)$$

For a simple estimation one can assume 1 GeV electron energy, which means  $\gamma = 2000$  and  $B\rho = 3.3$  Tm, and  $B_x = 10^5$  T magnetic field resulting in  $L_{cool} = \theta \times 0.6 \cdot 10^{-4}$  m. Even if we assume that  $\theta = 0.3$  radian, then  $L_{cool} = 20\mu\text{m}$ , which can be much shorter than the depletion length if the laser wavelength is short enough. This type of effective cooling should improve overall beam emittance as beam will continue accelerate as shown in Fig 8(e,f). Thus, the longitudinal magnetic field will acts not only to guide the electron beam (effective beam collimator) but also as a efficient coolant mediating conversion of beam transverse energy into high frequency synchrotron radiation at the same time.

### 3.2 The steady solenoid

So far the regime of large bubble is considered, where laser spot size  $W_L < \lambda_p$  and  $\lambda_{sp} < \lambda_p$ . In this case the magnetic field moves with the speed of light, constantly appears and disappears in the plasma, which might not be advantageous in some cases. If the pulse length approaches or

exceeds the bubble length more uniform magnetic field can be observed (see Fig. 5). This regime can be called as resonant regime when the plasma wavelength matches the spiral step of the laser pulse. If not only the pulse length, but the pulse width is also larger than the plasma wavelength a more efficient B-field generation is achieved. However in this case the bubble cannot be formed and as a result the spiral currents are not limited to a short intervals of bubble shell thus surviving over a longer distance behind the laser pulse.

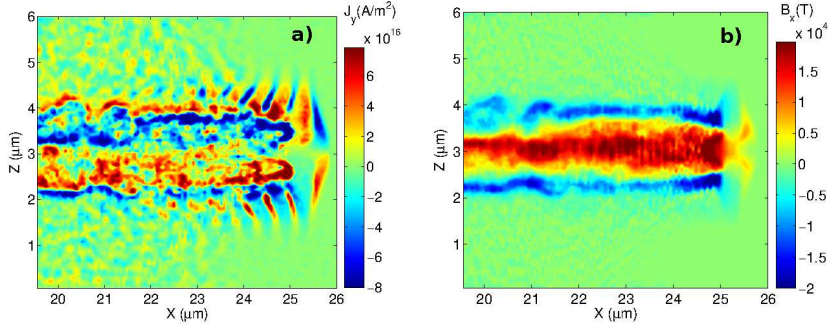


Figure 9: **(a)** Transversal current density and **(b)** longitudinal magnetic field are shown for the parameters:  $\lambda_{sp} = 0.9\mu\text{m}$ ,  $I_0 = 4 \times 10^{20}\text{W/cm}^2$ ,  $n_0 = 0.062n_{cr}$ ,  $W_L = 1.2\mu\text{m}$  and  $\lambda_L = 100\text{ nm}$ .

One example is presented in Fig. 9a and b, where it is shown that the longitudinal magnetic field is generated by the current density component perpendicular to the plane. The periodicity of stripes in the  $J_y$  distribution near the edges of the laser pulse shows that the plasma wavelength is about  $0.4\mu\text{m}$ , which is smaller than the pulse size. In that region the magnetic field is zero because the opposite currents cancel out each other, but in the channel behind the laser pulse the positive and negative magnetic fields are parallel and separated as expected in any solenoid structures. This structure brakes in the limit of  $W_L \gg \lambda_p$ , because of magnetic filaments evolving in the plasma if the current flow is wider than the local Debye-length. Therefore the pulse width should not be much larger than the plasma wavelength for optimal field generation.

The lifetime of magnetic fields generated in this way depends on the collision frequency between electrons and ions and on the magnetic diffusion time, which is defined as [23]  $t_d = \mu_0 R^2 / \eta$ , where  $R$  is the transverse scale length of the electron beam and  $\eta$  is the resistivity. The first effect is negligible in gases, but if  $>kT$  magnetic fields are generated, the plasma density could be high enough to smear out the electron rotation. The second effect is also negligible, because the plasma resistivity is on the order of  $10^{-6}\Omega\text{m}$ , which gives more than 100 fs diffusion time with  $R \approx 0.5\mu\text{m}$ . If one assumes that the laser pulse does not lose significant amount of energy during 100 fs the length of the quasi-static axial magnetic field can reach the sub-millimeter level.

## 4 Conclusions and outlook

We suggested and discussed the possibility of generating GigaGauss level axial magnetic field in underdense plasmas in laboratory environment using screw-shaped intense laser pulses. Generation of such a strong magnetic field is unprecedented at the current stage of state of the art technologies and if realized it could stimulate and motivate a number of new experimental campaigns now and in the near future. At lower density plasmas (gas) the usual  $\lambda_L \approx 1\mu\text{m}$  high power lasers (available to the researchers nowadays) are suitable for reaching the 10s of kT fields for a short period of time. It has been demonstrated that by changing the relative laser beam size with respect to the plasma wavelength the shape of the axial magnetic field distribution can be tuned. If the ratio of  $\lambda_p/\lambda_{sp}$  is near one, then a static solenoid magnetic field is generated along a straight line behind the laser pulse limited only by the laser pulse energy depletion. If the plasma wavelength is relatively large a bubble is formed and at its tail a strong, highly peaked and localized magnetic field is generated. This regime becomes non-linear (i.e. the introduced scaling does not work)

and unstable if the bubble size is too large and the charge of captured electrons influences the longitudinal electric and magnetic fields.

We note that the stable and repetitive production of screw-shape laser pulse still requires large amount of theoretical and experimental work in the field of laser physics. However, we believe that using such a laser pulse can bring a numerous advantages to the fields of laser wake field acceleration and astrophysics. This high magnetic field strength often observed in exotic cosmological objects, which also radiate in a wide range of x-ray and gamma frequency. The observation of radiation in PIC simulations requires very large resolution, which is inadmissible with the current high performance computing units. However, we can anticipate that the spiral motion of well-bunched relativistic electron beam will result in coherent synchrotron emission with high intensity at nm wavelengths.

Immersing electron bunches which are accelerated during laser plasma interaction into co-propagating axial magnetic field enable unique possibility to confine high density beam while improving beam emittance through synchrotron radiation cooling. We have demonstrated that large accelerating potential can be achieved simultaneously with strong longitudinal magnetic field at the point of beam self-injection. Showing that it is possible to use such accelerating structure will motivate future studies in this direction and in particular the investigation of transversal cooling of electrons due to synchrotron radiation and the effect of non-uniform axial B-field, which can behave as a magnetic mirror allowing to observe such phenomena as beam reflection and trapping. The possibility of using screw-shaped relativistic electron beams instead of laser pulses is also one of the follow-up research topics triggered by this work.

### **Acknowledgement:**

We would like to thank the developer team of Tech-X Corporation for the help and support in solving the issues regarding the parallel performance of the simulation code (VSim). The high performance computer cluster was provided by the John Adams Institute (Oxford). The ELI-ALPS project (GOP-1.1.1.-12/B-2012-0001, GINOP-2.3.6-15-2015-00001) is supported by the European Union and co-financed by the European Regional Development Fund.

## References

- [1] E. G. Zweibel, C. Heiles, Magnetic fields in galaxies and beyond, *Nature* **385**, 131–136 (1997)
- [2] J. Faure, Y. Glinec, et al., A laserplasma accelerator producing monoenergetic electron beams, stimulating coherent radiation, *Nature* **431**, p.541 (2004)
- [3] B. A. Remington, R. P. Drake, D. D. Ryutov, Experimental astrophysics with high power lasers and Z pinches, *Rev. Mod. Phys.* **78**, 755 (2006)
- [4] L. R. Elias, W. M. Fairbank, J. M. J. Madey, H. A. Schwettman, and T. I. Smith, Observation of Stimulated Emission of Radiation by Relativistic Electrons in a Spatially Periodic Transverse Magnetic Field, *Phys. Rev. Lett.* **36**, p.717 (1976)
- [5] Spruit, H. C. and Phinney, E. S., Birth kicks as the origin of pulsar rotation, *Nature* **393**, 139 (1998)
- [6] G. Gregori et al., Generation of scaled protogalactic seed magnetic fields in laser-produced shock waves, *Nature* **481**, 480483 (2012)
- [7] Balandina, A.N., et. al., Magnetic Field Generation and Related Topics (MEGAGUSS), 2012 14th International Conference on Megagauss, IEEE 2012, pp.1-7
- [8] V. K. Chernyshev, V. D. Selemir, and L. N. Plyashkevich, Super-power explosive magnetic sources for thermonuclear and physical research, in Megagauss and megaampere pulsed technology and application, Eds. Sarov: RFNC-VNIIEF, pp. 4158. (1997)
- [9] S. V. Lebedev, et al., X-ray backlighting of wire array Z-pinch implosions using X pinch, *Rev. Sci. Instrum.* **72**, 671 (2001)
- [10] P. J. Turchi, A. L. Cooper, R. D. Ford, D. J. Jenkins, and R. L. Burton, Review of the NRL Liner Implosion Program, *Megagauss Physics and Technology*, Ed. Peter Turchi, Plenum Press, New York (1980)
- [11] J. Slough, A. Pancotti, D. Kirtley, Magnetic Field Generation and Related Topics (MEGAGUSS), 2012 14th International Conference on Megagauss, 2012
- [12] Sims, J.R. ; Rickel, D.G. ; Swenson, C.A. ; Schillig, J.B. ; Ellis, G.W. ; Ammerman, C.N., Assembly, Commissioning and Operation of the NHMFL 100 Tesla Multi-Pulse Magnet System, *IEEE Transactions on Applied Superconductivity* **18**, p.587-591 (2008)
- [13] Naseri, Bychenkov, and Rozmus, Axial magnetic field generation by intense circularly polarized laser pulses in underdense plasmas, *Phys. Plasmas* **17**, 083109 (2010)
- [14] Zs. Lecz and A. Andreev, Attospiral generation upon interaction of circularly polarized intense laser pulses with cone-like targets, *Phys Rev E* **93**, 013207 (2016)
- [15] Yin Shi et al., Light Fan Driven by a Relativistic Laser Pulse, *Phys Rev Lett* **112**, 235001 (2014)
- [16] Zs. Lecz, A. Andreev and A. Seryi, Plasma rotation with circularly polarized laser pulse, *Laser and Particle Beams* **34**, 31-42 (2015)
- [17] J. Vieira et al., Amplification and generation of ultra-intense twisted laser pulses via stimulated Raman scattering, *Nature Communications* **7**, 10371 (2016)
- [18] T. Antonsen and P. Mora, Kinetic modeling of intense, short laser pulses propagating in tenuous plasmas, *Phys. Plasmas* **4**, 217 (1997)

- [19] D. Gordon, W. Mori, and T. Antonsen, Jr., A Ponderomotive Guiding Center Particle-in-Cell Code for Efficient Modeling of LaserPlasma Interactions, *IEEE Trans. Plasma Science* **28**, 11351143 (2000)
- [20] P. Messmer and D. L. Bruhwiler, Simulating laser pulse propagation and low-frequency wave emission in capillary plasma channel systems with a ponderomotive guiding center model, *Phys. Rev. ST Accel. Beams* **9**, 031302 (2006)
- [21] E. Esarey et al., Physics of laser-driven plasma-based electron accelerators, *Review of Modern Physics* **81**, 1229 (2009)
- [22] J. D. Jackson, *Classical Electrodynamics*, 3rd ed. (Hamilton, New York, 1999)
- [23] J.R. Davies, Electric and magnetic field generation and target heating by laser-generated fast electrons, *Physical Review E* **68**, 056404 (2003)

## Appendix

The laser pulse shape is rather complicated and for stable pulse propagation the condition  $\lambda_L \ll \lambda_{sp}$  should be fulfilled. Furthermore we are interested in the regime where  $\lambda_p \gg \lambda_{sp}$ . Since the laser wavelength is the smallest spatial scale length to be resolved, the number of grid cells would be way too large (on the order of  $1000 \times 1000 \times 1000$ ) for 3D simulations. Therefore a model optimization should be used in order to make the numerical studies feasible. It is well known that instead of defining the laser field it is possible to propagate the intensity distribution itself, and by calculating its gradient, an effective force-field acting on the plasmas can be evaluated. This approach (known as envelope approximation) is sufficient to model the electron motion in the plasma and using it one needs to resolve only the laser pulse envelope function, which requires much lower spatial resolution. With this approximation the grid mesh can be 10 times courser, thus the simulation time and amount of data 1000 times less.

Although the fast oscillations of the electromagnetic field in the laser pulse are not modeled, the laser frequency remains an important parameter which defines the critical plasma density. In the equation of motion the source terms are the electric ( $E$ ) magnetic ( $B$ ) fields, which appear as a cross product. The modulus of the resulting vector Poynting,  $\mathbf{S} = \mathbf{E} \times \mathbf{B}/\mu_0$ , has physical meaning of the intensity of the pulse. If we assume that  $\mathbf{S}$  points only in the forward direction it is possible to replace it with the scalar field of intensity (i. e. projection of  $\mathbf{S}$ ), which represents the source term of the equation of motion and its gradient defines the ponderomotive force:

$$F = \frac{e^2}{4m_e\omega_L^2\epsilon_0 c} \nabla I_L, \quad (3)$$

where  $I_L(x, y, z)$  is a three dimensional function. To couple this force-field to the electrons in the code we need to define this force-field  $F$  via an effective electric field. This effective electric field can be evaluated by dividing  $F$  by the elementary charge and thus observing the corresponding electric field acting on the charged particles. This effective pusher field acts as an external field and it is not included in the Maxwell solver, but it is added to the self-generated electric field before the particle pusher algorithm solves the relativistic equation of motion. The detailed comparison between the simulation with the real and envelope pulse can be found in the supplementary material, where good agreement can be seen.

The cork-screw shape of the laser envelope can be obtained by implementing a rotating elliptic beam profile, with periodicity  $\lambda_{sp}$ . The transverse beam profile at one point of the pulse is the superposition of two Gaussian shapes: one is rotation symmetric with standard deviation  $\sigma_1$  and one is uniform in the radial direction with  $\sigma_2 < \sigma_1$  in the orthogonal direction. After some geometric calculations one can derive the function of a line rotating around the axis in the transverse plane, which will give the radial direction of the second Gaussian. Finally, the function describing the intensity distribution has the the following form:

$$I_L = I_0 \exp\left(-\frac{D^2}{2\sigma_2^2}\right) \exp\left(-\frac{r^2}{2\sigma_1^2}\right) \cos[(2x/L_{lp} - 1)\pi/2], \quad (4)$$

where  $L_{lp}$  is the total pulse length,  $r = \sqrt{y^2 + z^2}$  and the distance from the rotating line in the transverse plane:

$$D(x, y, z) = [(y - \cos(\alpha)(z \tan(\alpha) + y))^2 + (z - \sin(\alpha)(z \tan(\alpha) + y))^2]^{1/2}, \quad (5)$$

where  $\alpha = \pi x/\lambda_{sp}$  is the phase of the spiral envelope. In Eq. 4 a cosine function also appears, which is the longitudinal envelope. The usual Gauss function is not appropriate in this case, because it has to be truncated and the gradient at the leading edge of the pulse would be too large. By using this function we can assure that the intensity value is zero at both ends of the pulse.

In the simulation the above derived expression is propagated in the  $x$  direction, which means that in the argument of the cosine  $x$  is replaced by  $x - ct$  and at each time step the intensity

distribution is shifted by the grid size,  $dx$ . In this method the energy depletion of the pulse is not included, the energy content of the pulse does not change. This propagation gives unrealistic result after a long distance, but on our time scale of interest ( $< 100$  fs) and in under-dense plasmas ( $n_0 < 0.1n_{cr}$ ) the infinite energy source is a reasonable assumption.

The simulations are performed using the fully relativistic 3D VSim particle-in-cell (PIC) code. The simulation space contains  $300 \times 300 \times 300$  computational mesh cells with variable grid sizes depending on the bubble size. The propagation time is about 100 fs, which corresponded to about 2000 PIC cycles. The plasma is represented by electrons with under-critical density with 5 macro-particles in each cell. In order to simulate propagation distance much longer than the domain size we applied the moving window feature of the VSim code. In this case the simulation box is moving in the positive  $x$  direction with the speed of light and in each time step electrons are loaded in the new grid cell appearing at the front side and electrons are absorbed at the back side of the simulation domain.

In one time step, beside the usual Maxwell solver, the code performs the gradient calculation of the scalar field defined by Eq. 4. The vector field obtained this way is converted into electric field and added to the self field generated by the charge of electrons. In this way the electrons respond to the acting field of the laser pulse and the self-consistency is also preserved. The only thing, which might be not resolved by the spatial mesh is the motion of the electron beam. The Larmor radius of the electron trajectory can be smaller than 10 nm, but our grid size is typically 20-30 nm, or larger.